

Published in final edited form as:

J Am Chem Soc. 2009 September 9; 131(35): 12780–12791. doi:10.1021/ja9041077.

The role of nanoparticle valency in the nondestructive magnetic-relaxation-mediated detection and magnetic isolation of cells in complex media

Charalambos Kaittanis^{‡, #}, Santimukul Santra[‡], and J. Manuel Perez^{‡, #, *}

[‡]Nanoscience Technology Center, University of Central Florida, 12424 Research Parkway, Suite 400, Orlando, FL 32826

[#]Burnett School of Biomedical Sciences – College of Medicine, University of Central Florida, 12424 Research Parkway, Suite 400, Orlando, FL 32826

^{*}Department of Chemistry, University of Central Florida, 12424 Research Parkway, Suite 400, Orlando, FL 32826

Abstract

Nanoparticle-based diagnostics typically involve the conjugation of targeting ligands to the nanoparticle in order to create a sensitive and specific nanosensor that can bind and detect the presence of a target, such as a bacterium, cancer cell, protein or DNA sequence. Studies that address the effect of multivalency on the binding and detection pattern of these nanosensors, particularly on magnetic relaxation nanosensors that sense the presence of a target in a dose-dependent manner by changes in the water relaxation times (ΔT_2), are scarce. Herein, we study the effect of multivalency on the detection profile of cancer cells and bacteria in complex media, such as blood and milk. In these studies, we conjugated folic acid at two different densities (low-folate and high-folate) on polyacrylic-acid-coated iron oxide nanoparticles and studied the interaction of these magnetic nanosensors with cancer cells expressing the folate receptor. Results showed that the multivalent high-folate magnetic relaxation nanosensor performed better than its low folate counterpart, achieving single cancer cell detection in blood samples within 15 minutes. Similar results were also observed when a high molecular weight anti-folate antibody (MW: 150 kDa) was used instead of the low molecular weight folic acid ligand (MW: 441.4), although better results in terms of sensitivity, dynamic range and speed of detection were obtained when the folate ligand was used. Studies using bacteria in milk suspensions corroborated the results observed with cancer cells. Taken together, these studies demonstrate that nanoparticle multivalency plays a key role in the interaction of the nanoparticle with the cellular target and modulate the behavior and sensitivity of the assay. Furthermore, as detection with magnetic relaxation nanosensors is a non-destructive technique, magnetic isolation and further characterization of the cancer cells is possible.

Nanoscience Technology Center, University of Central Florida, 12424 Research Parkway, Suite 400, Orlando, FL 32826. Ph: 407-882-2843. Fax: 407-882-2819. jmperez@mail.ucf.edu.

Valency-mediated interactions between magnetic nanoparticles and cells

SUPPORTING INFORMATION PARAGRAPH. (1) Nanoparticle characterization, (2) DLS of bacterial nanosensors, (3) correlation coefficients of time-dependent magnetic relaxation studies, and (4) determination of the expression of folate receptor via flow cytometry. This material is available free of charge through the World Wide Web at <http://pubs.acs.org>.

Introduction

The enhanced binding of multiple ligands to a particular cellular target is a common approach in nature to fine-tune molecular and cellular recognitions with increased specificity.¹⁻¹¹ This kind of multivalent binding strategy can offer unique advantages for developing selective and highly sensitive nanoparticle-based diagnostics and effective therapeutics. Nanoparticles with multiple targeting ligands offer the advantage of a surface-mediated multivalent affinity, resulting from multiple interactions between the high local concentration of binding ligands on the nanoparticle's surface and epitopes on the corresponding target. In particular, the conjugation of multiple targeting ligands to iron oxide nanoparticles (IONP) has allowed the creation of multivalent magnetic relaxation nanosensors (MRnS) for the detection of molecular targets and events, such as DNA, RNA, proteins, enzymatic activity, small molecule, viruses, enzymatic and metabolic activity.¹²⁻¹⁶ Detection is achieved by changes in the solution's water relaxation times (ΔT_2), as these nanosensors self-assemble upon interaction with the specific target. However, all these cases shared a common target characteristic; the target was smaller than or had roughly the same size (in the case of a virus) with the nanosensor. Recently, the detection of a bacterium, a much larger target compared to the nanosensor, was reported.¹⁷ In that report, it was found that the use of a multivalent entity (bacterium) as a biological target compensated for the size difference between the nanoprobe and the target, promoting nanoparticle assembly on the bacterial surface with concomitant target-concentration-dependent changes in ΔT_2 . It was speculated that these differences may have been attributed to the ratio of nanoparticles interacting per target, hinting that at low bacterial concentrations more nanoparticles self-assembled on the surface of the bacterium (hence higher ΔT_2), whereas at high bacterial concentrations fewer nanoparticles interacted per target to result in lower ΔT_2 .

Therefore, we hypothesized whether the nanoparticles' valency may affect the MRnS detection limit, allowing the engineering of ultrasensitive probes to accommodate a particular cellular concentration range. We reasoned that nanoparticles with low amounts of ligand conjugated on their surface (low valency) would assemble on the cell's surface, resulting in prominent shifts in the ΔT_2 (Scheme 1A). As the cell concentration increases, the low valency nanoparticles would switch to a quasi-dispersed state, due to their limited interaction with target moieties on discrete cells, thus causing smaller changes in the ΔT_2 at high cell concentrations (Scheme 1A). This mechanism would be in line with the reported MRnS-mediated detection of bacteria (*Mycobacterium avium* spp *paratuberculosis* – MAP) using magnetic nanoparticles conjugated with anti-MAP polyclonal antibodies, where prominent ΔT_2 was observed at low MAP amounts and low ΔT_2 was recorded at high MAP concentrations.¹⁷ In contrast, we reasoned that high valency nanoparticles should not cluster in the presence of cells at low concentrations. Instead, the multiple ligands present on the high valency nanoparticle can interact with multiple receptors on the cell surface (Scheme 1B). Therefore, the interaction between high valency nanoparticles and cells at low concentration would result in a less pronounced ΔT_2 , because a fewer number of nanoparticles may simultaneously interact with multiple receptors in a given cell. Alternatively, as the cell concentration increases, the probability of high valency nanoparticle binding to surface receptors in multiple cells increases. This should facilitate the binding of multiple ligands on the same nanoparticle with multiple receptors on different cells, causing extensive clustering of the nanoparticles and an increase in ΔT_2 as the number of cells increases. (Scheme 1B).

Hence, the lack of a comprehensive study addressing how multivalency affects the nanoparticles' cell surface assembly (e.g. bacterium or cell) and the corresponding MRnS response prompted us to utilize MRnS with engineered valency towards the detection of cancer cells in blood samples. We selected cancer cells as a model target, because it has been recently reported that viable tumor-derived epithelial cells found in circulation (circulating tumor cells)

are a novel class of cancer biomarkers, participating in the initiation of the process of metastasis.¹⁸⁻²⁰ Current molecular diagnostic techniques cannot detect low concentrations of cells in complex media (i.e. blood),²⁰ because of the matrix's optical properties and complexity. Furthermore, commonly used cytological and immunocytochemical techniques require the cell's isolation, purification, fixation and quantification using fluorescent probes and microscopic examination, which prevent propagation of the cells for further analyses.^{21,22} All of the above highlight the importance of developing nondestructive methods for the sensitive detection of circulating tumor cells in blood samples. For our studies, we decided to use a small molecule as opposed to an antibody, because its small size could guarantee higher nanoparticle multivalency and its stability would lead to the development of robust field-deployable nanosensors that are not susceptible to thermal denaturation. As a model small molecule ligand, we chose folic acid (folate), which is the canonical affinity ligand of the folate receptor (FR) that is overexpressed in some tumor cells.²³ Although circulating tumor cells more prevalently overexpress other cell surface markers, such as EpCAM,¹⁹ recent studies indicate that the folate receptor (FR) is overexpressed in numerous cancers, including ovarian, testicular, breast and lung.²³ Furthermore, as the expression of FR is upregulated during metastasis, this receptor is a good marker for diagnosis, targeted imaging and drug delivery. As our cellular target, we used A549 lung cancer cells, as lung cancer is among the most common sites of origin of metastatic cancer through migration of lung cancer cells via the circulation,²⁴ and this cell line is known to overexpress the folate receptor.²³ Therefore, we investigated if the folate nanoparticle preparations, and particularly the high-folate ones, can be used for the quantification and sensitive detection of single FR-expressing A549 cells in complex media, via magnetic relaxation. Results showed that low valency nanoparticles at low target concentrations induced high ΔT_2 , whereas at high cell concentrations the nanoparticles switched to a dispersed-like state with lower ΔT_2 values. Corresponding dynamic light scattering (DLS) analysis and cell associated fluorescence studies confirmed these results. On the other hand, high valency nanoparticles from a disperse-like state switched to a clustered state, when we increased the cell concentration. Similar observations were made when we used low and high valency nanoparticles for the detection of bacterial cells, indicating that the interaction was modulated by the nanoparticle valency and not the targeted cell. Furthermore, results show that the high valency nanoparticles performed better than their low valency counterpart as they achieve a high sensitivity, faster detection kinetics and more efficient magnetic isolation of cells for subsequent analyses. Hence, considering the need for circulating cancer cell diagnostic modalities, herein we demonstrate that multivalent iron oxide nanosensors, carrying a small affinity ligand, can facilitate (i) fast detection of tumor cells in blood via magnetic relaxation, (ii) the magnetic isolation and propagation of these cells for further analyses, and (iii) the cells' colorimetric identification via the nanoparticles' intrinsic peroxidase activity. The same approach can be expanded to the detection of other cells in circulation, as well as pathogens.

Experimental Section

Materials

All reagents were of AR (Analytical Reagent) grade. Iron salts ($\text{FeCl}_2 \cdot 4\text{H}_2\text{O}$ and $\text{FeCl}_3 \cdot 6\text{H}_2\text{O}$) were obtained from Fluka. Polyacrylic acid (MW 1.8 kDa), ammonium hydroxide, hydrochloric acid, folic acid, N, N'-dimethylformamide (DMF), N-hydroxysuccinimide (NHS) and 3-(4,5-Dimethylthiazol-2-yl)-2,5-diphenyltetrazolium bromide (MTT) were purchased from Sigma-Aldrich. The dialkylcarbocyanine fluorophore DiI (D282) and the nuclear stain DAPI (4', 6-diamidino-2-phenylindole – D1306) were purchased from Invitrogen. EDC (1-Ethyl-3-[3-dimethylaminopropyl] carbodiimide hydrochloride) and Protein G were obtained from Pierce Biotechnology, whereas the polyclonal rabbit anti-human folate receptor antibody (FL-257) was purchased from Santa Cruz

Biotechnology. The polyclonal anti-MAP antibody was a gift from Dr. Saleh Naser (Burnett School of Biomedical Sciences, College of Medicine, UCF).

Synthesis of propargylated polyacrylic-acid-coated iron oxide nanoparticles

The polyacrylic-acid-coated iron oxide nanoparticles were synthesized using the alkaline precipitation method, as recently reported.²⁵ Briefly, the nanoparticles were prepared by rapidly mixing a $\text{Fe}^{+3}/\text{Fe}^{+2}$ solution with an ammonium hydroxide solution for 30 seconds, before adding the polyacrylic acid (PAA) solution. The nanoparticles were washed, concentrated and finally reconstituted in phosphate buffered saline (pH = 7.4), using a KrosFlo Research II TFF system equipped with a 10kDa column (Spectrum Labs). Propargylation of the as synthesized nanoparticles was achieved with carbodiimide chemistry, as previously reported.²⁵ The propargylated nanoparticles were magnetically separated and characterized, following published protocols.²⁵

Synthesis of folate-carrying nanoparticles with different nanoparticle valency using “click” chemistry

To synthesize folate-conjugated nanoparticles, propargylated nanoparticles (13 mg, 1.69 mg/mL) were added to azide-functionalized folic acid (folate- N_3), according to the literature.²⁵ Different levels of nanoparticle valency were achieved by varying the stoichiometric ratio of nanoparticle ligand to nanoparticle concentration. For the preparation of low-folate nanoparticles, 0.4 g of folic acid (0.8×10^{-2} μmol) were used, whereas for the high-folate nanoparticles 4 mg (8×10^{-2} mmol) of folic acid in DMSO. The reaction was initiated at room temperature in the presence of catalytic amount of CuI (0.01 μg , 0.6×10^{-10} mmol), in 125 μL of bicarbonate buffer (pH 8.5), and further incubated for 12 h at room temperature (“click” chemistry). The final reaction mixture was purified with a magnetic column, and finally dialyzed using a 6,000 – 8,000 MW cutoff dialysis bag, against deionized water and phosphate buffered saline (PBS) solution. The folate nanoparticle preparations were stored at 4 °C until further use. Confirmation of the successful conjugation of folate to the nanoparticles was achieved through UV-Vis and fluorescence emission spectroscopy. In order to make our nanoparticles multimodal, we loaded them with a lipophilic fluorophore. Dye-doped folate-conjugated iron oxide nanoparticles were prepared by the drop-wise addition of DiI (0.1 $\mu\text{g}/\mu\text{L}$ in DMF) in 4.5 mL of the nanoparticle suspension ($[\text{Fe}] = 1.69 \text{ mg/mL}$), as described in literature.²⁵ The nanoparticles were magnetically separated, and the complete removal of free (non-encapsulated) dye was confirmed through fluorescence emission spectroscopy, demonstrating a single red-shifted emission maximum. Finally, the nanoparticles were stored in dark at 4 °C until further use.

Synthesis of antibody-carrying nanoparticles with different nanoparticle valency

For the conjugation of Protein G to the nanoparticles, polyacrylic-acid-coated nanoparticles ($[\text{Fe}] = 0.25 \text{ mg/mL}$) were taken in 2 mL MES buffer (pH = 6), and to this we added EDC (1 mg, 0.11 mmol) and NHS (0.8 mg, 0.15 mmol). This reaction mixture was incubated for 3 minutes, followed by drop-wise addition of Protein G (1.5 mg, 60 μmol) in DI water (0.5 mL). Next, the solution was incubated for 30 min at room temperature under continuous mixing, followed by overnight incubation at 4 °C. In order to remove any Protein G molecules that did not conjugate to the nanoparticles, we performed magnetic separation using a 1X-PBS-equilibrated LS25 column. Protein quantification revealed that the nanoparticle preparation's Protein G concentration was 0.1 $\mu\text{g}/\mu\text{L}$. Subsequently, we conjugated either anti-FR or anti-MAP antibodies to the Protein G-carrying nanoparticles, as previously reported.¹⁶ However, in order to engineer the nanoparticle valency, the Protein G nanoparticles (250 μL) were incubated with different antibody amounts (5 μg anti-FR, 0.5 ng anti-FR, 5 μg anti-MAP or

0.5 ng anti-MAP), yielding either anti-FR or anti-MAP nanoparticles with different degrees of valency, which was assessed in accordance to the literature.^{26,27}

Nanoparticle characterization

The size of the folate-conjugated iron oxide nanoparticles was determined through dynamic light scattering (DLS), using a PDDLS CoolBatch 40T instrument and the Precision Deconvolve 32 software. Iron concentration was determined spectrophotometrically after acid digestion of the nanoparticles' suspension as previously reported,^{25,28} whereas r_1 and r_2 relaxivity measurements were obtained using a 0.47T mq20 NMR analyzer (Minispec, Bruker, Germany). Zeta potential measurements were performed on a Nano-Z zetasizer (Malvern), operating at 25 °C. To determine the presence of propargyl groups on the surface of the propargylated nanoparticles, FT-IR was performed on a PerkinElmer Spectrum 100 FT-IR spectrometer, and to confirm the successful conjugation of folate to the folate nanoparticles' surface UV-Vis absorbance and fluorescence emission profiles were obtained, using a Cary300 spectrophotometer (Varian) and a NanoLog-3 fluorimeter (Horiba Jobin-Yvon). Similarly, the folate nanoparticles' fluorescence emission associated with the encapsulated DiI was determined with the NanoLog-3 fluorimeter. Protein G and antibody quantification was achieved colorimetrically through the BCA assay (Pierce) in accordance to the supplier's protocol, and determination of the amount of folate and antibody per nanoparticle was determined as described in literature.^{16,26,27}

Mammalian cell studies

Cell cultures—Cancer human alveolar cells (A549) and normal (non-cancer) rat cardiomyocytes (H9c2) were obtained from ATCC, and maintained in accordance to the supplier's protocols. Briefly, the A549 cells were maintained in a 5%-FBS-containing DMEM medium supplemented with antimycotic/antibiotic, whereas the H9c2 cells were propagated in a 10%-FBS-containing MEM medium containing antimycotic/antibiotic. All cell cultures were grown in a humidified incubator at 37 °C under a 5% CO₂ atmosphere.

Hemocytometer-mediated cell quantification—After detaching the cells from the culture plate using trypsin and suspending them in growing medium, the cellular suspension was centrifuged at 1,000 rpm for 8 minutes and the pellet was re-suspended in 2 mL of the corresponding medium. Ten μ L aliquots of the resulting cell suspensions were thoroughly mixed with 10 μ L trypan blue solutions. Quantification was performed using a hemocytometer and a phase-contrast microscope.

Serial dilutions of stock cellular suspensions—After determining the cell concentration of the stock suspensions, serial dilutions were prepared in 1X PBS, 5% PBS-diluted blood or whole blood, using aseptic techniques. Fresh blood was a gift from Dr. James Hickman (UCF NSTC), obtained from bacteremia-free Crl:CD(SD)IGSBR female rats (Charles River Laboratories). All serial diluted samples were used immediately after preparation.

Fluorimetry-based determination of nanoparticles – cell association—One mL cellular suspensions (10^3 and 10^6 A549 cells) in PBS, were incubated with 1 μ L folate-carrying nanoparticles ($[\text{Fe}] = 1.69 \mu\text{g/mL}$) for 60 minutes at room temperature, under continuous mixing (300 rpm). To remove any unbound nanoparticles, the samples were centrifuged three times at 1,000 rpm for 8 minutes, each centrifugation round followed by washing with 1X PBS. The resulting cell pellets were resuspended in 1 mL 1X PBS, and fluorescence emission spectra were recorded using a NanoLog-3 fluorimeter (Horiba Jobin-Yvon).

Confocal laser-scanning microscopy—A549 cells were grown overnight on culture dishes, before treatment. After incubation with the nanoparticles, the cells were washed three times with 1X PBS, fixed with 5% formalin solution, and stained with DAPI (Molecular Probes). Subsequently, the cells were examined with a Zeiss LSM 510 confocal microscope equipped with a 40X objective.

Dynamic light scattering (DLS)—One mL cellular suspensions in PBS, either with 10^3 or 10^6 A549 cells, were incubated with 1 μ L folate-PAA-IONP ($[\text{Fe}] = 1.69 \mu\text{g/mL}$) for 60 minutes at room temperature, under continuous mixing (300 rpm). The alterations in the nanoparticle size distribution were monitored through the PDDLS CoolBatch 40T instrument and the Precision Deconvolve 32 software.

Magnetic-relaxation-mediated cell detection—Ten μ L aliquots of cell suspensions were incubated with 190 μ L of nanoparticle working solutions ($[\text{Fe}] = 0.01 \mu\text{g}/\mu\text{L}$) at room temperature. Spin-spin relaxation times (T_2) were recorded over time via the 0.47T mq20 NMR analyzer (Minispec, Bruker, Germany), operating at 40 °C.

Magnetic isolation of A549 cells and detection of the expression of the folate receptor—After screening samples via magnetic relaxation, they were incubated with various concentrations of folate-PAA-IONP for 30 minutes at 37 °C. Subsequently, each sample was passed through a 1X-PBS-equilibrated LS25 MACS[®] column (Miltenyi Biotec). After removing the column from the magnet, the eluate was captured in culture dishes with 5%-FBS-containing DMEM medium. The dishes were placed in a humidified incubator (37 °C, 5% CO_2) for 24 h, as according to the supplier the doubling time of A549 cells is 18 h. Then, the cells were washed three times with 1X PBS and fresh medium was added. Cells were quantified using the hemocytometer method and 500-cell aliquots of either A549 or H9c2 cells were seeded into a 96-well microtiter plate. After overnight growth, the cells were incubated for 1 h with different nanoparticle concentrations at 4 °C. Then, the cells were washed three times with 1X PBS in order to remove any unbound nanoparticles, and 100 μ L of 0.2 mM TMB in citrate buffer pH 4.0 (3, 3', 5, 5'-tetramethylbenzidine, Sigma) as well as 10 μ L H_2O_2 (Acros) were added. Twenty minutes after absorbance was recorded at 652 nm, using a μ Quant 200 microtiter plate reader (Biotek).

Flow cytometry—A549 and H9c2 cells were grown until reaching confluence. After detachment and centrifugation at 1000 rpm, the cell pellets were collected and resuspended in 1X PBS. The resulting cell suspensions were incubated with the anti-folate-receptor antibody (0.5 $\mu\text{g/mL}$) for 30 min at 4 °C, under continuous mixing. After the incubation with the primary antibody, the cells were centrifuged and resuspended in PBS three times, followed by a 30-min incubation at 4 °C with an FITC-conjugated goat anti-rabbit-IgG antibody (0.5 $\mu\text{g/mL}$). The FITC-conjugated antibody was a gift from Dr. James Hickman (Nanoscience Technology Center, UCF). Finally, the cells were centrifuged and resuspended in PBS three times, and the cellular suspensions were examined using a FACSCalibur flow cytometer (BD Biosciences).

Cell viability studies—Equal populations of A549 cells either magnetically isolated using the folate-carrying iron oxide nanoparticles or readily harvested, which had been quantified with a hemocytometer, were seeded in 96-well plates. After overnight growth in a 5%-FBS-containing DMEM medium at 37 °C, 5% CO_2 in a humidified incubator, the cells were washed three times with 1X PBS and treated with 20 μ L MTT (5 $\mu\text{g}/\mu\text{L}$, Sigma-Aldrich) for 2 hours. Using acidified isopropanol (0.1 N HCl), the formazan crystals were dissolved and the absorbance was recorded at 570 nm and 750 nm (background) via a Synergy μ Quant microtiter plate reader (Biotek).

Bacterial cell studies

Bacterial stocks—Serial dilutions of heat inactivated *Mycobacterium avium* spp. *paratuberculosis* (MAP) in 1X PBS and anti-MAP antibody were a gift from Dr. Saleh Naser (Burnett School of Biomedical Sciences, College of Medicine, UCF).

Magnetic-relaxation-mediated bacterial cell detection—Similar to the mammalian cell (A549) protocol, ten μL aliquots of cell suspensions were incubated with 190 μL of nanoparticle working solutions ($[\text{Fe}] = 0.01 \mu\text{g}/\mu\text{L}$) at room temperature. Spin-spin relaxation times (T_2) were recorded over time via the 0.47T mq20 NMR analyzer (Minispec, Bruker, Germany), operating at 40 °C.

Dynamic light scattering (DLS)—Similar to the corresponding mammalian studies, one mL MAP bacterial suspensions in PBS, either with 500 or 5 CFUs (Colony Forming Units), were incubated with 1 μL anti-MAP-PAA-IONP ($[\text{Fe}] = 0.50 \mu\text{g}/\text{mL}$) for 60 minutes at room temperature, under continuous mixing (300 rpm). The alterations in the nanoparticle size distribution were monitored through the PDDLS CoolBatch 40T instrument and the Precision Deconvolve 32 software.

Data analysis: All experiments were performed at least three times, and during each experiment three measurements were taken for each experimental condition. Each graph dataset contains the obtained averages of the corresponding study. Total fluorescence intensity per mL (Total FI_{mL}) is defined as the summation of each 1-mL sample's fluorescence intensities from 570 to 640 nm. For the magnetic relaxation quantification plots, the best model fit was achieved using either linear or sigmoidal fit (OriginPro 7.5, Origin Lab Corp, MA, USA). As we previously reported, ΔT_2 is defined as the average $T_{2\text{sample},i}$ minus the average $T_{2\text{control},i}$ at time i , where for the control sample sterile, non-spiked medium (blood or milk) was used.¹⁷ To determine cell viability, we subtracted the background absorbance at 750 nm from the absorbance at 570 nm, as previously reported.²⁵ The percentage cell viability for the cells isolated was calculated using the formula: $\Delta A_{570-750\text{sample}}/\Delta A_{570-750\text{control}} \times 100$, where the corresponding control for the cells isolated with low- and high-folate nanoparticles were harvested cells seeded in low and high population counts (Control low and Control high).

Results

Synthesis of iron oxide nanoparticles with ligand-varying valency

To examine our hypothesis, we prepared polyacrylic-acid-coated iron oxide nanoparticles with different ligand valency by varying the stoichiometry of the conjugation reaction. These polymer-coated nanoparticles had an average hydrodynamic diameter of 90 nm, ζ potential of $-82.6 \pm 2.4 \text{ mV}$, spinlattice (r_1) and spin-spin relaxations (r_2) of $53 \text{ mM}^{-1}\text{s}^{-1}$ and $206 \text{ mM}^{-1}\text{s}^{-1}$, respectively. “Click” conjugation of targeting moieties to the nanoparticles' surface was achieved by incorporating alkyne groups via carbodiimide chemistry (SI Scheme 1 and SI Figure 1), having a ζ potential of $-62.6 \pm 2.9 \text{ mV}$. As a model targeting moiety, we used folic acid (MW: 441.4), which is the affinity ligand of the transmembrane folic acid receptor (FR) that is overexpressed in several cancers.²³ Hence, azide-functionalized folic acid was conjugated to the alkyne-carrying polyacrylic-acid-coated nanoparticles via click chemistry, having different concentrations of folate while maintaining constant the nanoparticle concentration. The presence of folate on the nanoparticles was corroborated by the presence of a 352 nm shoulder peak in the UV-Vis absorbance spectrum (SI Figure 2) and a corresponding 446 nm peak in the fluorescence emission spectrum (SI Figure 3). Using this spectrophotometric information and following published protocols,^{26,27} we determined that the high-folate nanoparticles had on average 120 folic acid moieties per nanoparticle (ζ potential = $-59.4 \pm 3.6 \text{ mV}$), whereas the low-folate nanoparticles had on average 1 folic acid

per nanoparticle (ζ potential = -53.5 ± 4.1 mV). The folate-carrying nanoparticles were then doped with the fluorophore (DiI), resulting in fluorescently labeled nanoparticles (SI Figure 4), as recently reported.²⁵ Contrary to fluorophore conjugation to the nanoparticles' surface, this method facilitates fluorophore encapsulation within the polymeric coating's microdomains and does not compromise the nanoparticles' folic acid valency, allowing the use of these nanoparticles in fluorimetric (Figure 1) and confocal microscopy studies with folate-receptor expressing cells (SI Figure 5).

In addition to the folate nanoparticles that carry a small molecule (folate), we synthesized nanoparticles with different levels of anti-folate-receptor (anti-FR) antibodies (MW: 150,000). Specifically, via carbodiimide chemistry, Protein G was conjugated to the as synthesized polyacrylic-acid-coated nanoparticles, which have readily available carboxylic acid groups. Following magnetic separation and nanoparticle-associated protein quantification (2 Protein G molecules per nanoparticle on average), the antibodies were conjugated to the Protein G nanoparticles through an overnight reaction carried at 4 °C. Specifically to engineer the valency and obtain nanoparticles with either low or high levels of conjugated antibodies, we varied the stoichiometry of the nanoparticle conjugation reaction, by modifying one of the reactant's concentration (either 5 μ g anti-FR or 0.5 ng anti-FR) while keeping the Protein G nanoparticles' amount constant (250 μ L). These conjugation reactions resulted in the formation of nanoparticles with high (4 anti-FR molecules per nanoparticle on average) and low (1 anti-FR molecule per nanoparticle on average) anti-FR levels, as determined with the BCA assay following literature available protocols.

Assessment of the ligand-modulated nanoparticle – mammalian cell interactions

To test our hypothesis, we first investigated the nanoparticle – cell associations via fluorescence spectroscopy. Since our nanoparticles apart from magnetic are fluorescent, we employed this technique due to its enhanced sensitivity and spectral acquisition capability, allowing the determination of the nanoparticle – cell association and quantification of this interaction by recording the fluorescence emission from the magnetically isolated folate-receptor expressing cells. Therefore, any fluorescence emission associated with the isolated cells should have been an indication of the degree of interaction between the nanoparticles' ligands and cell surface receptors. A major advantage of fluorescence spectroscopy in contrast to confocal laser scanning microscopy is its ability to determine the cell – nanoparticle interaction in suspension, where confocal microscopy requires adherent cells. Additionally, although flow cytometry is an alternative solution-based technique, it was not employed because (i) large cell populations are required to obtain statistically significant results, (ii) it has limited sensitivity for fluorophores that weakly associate with cells or at low fluorophore concentrations (for instance few nanoparticles), and (iii) the compromised multispectral capability (restricted number of acquired wavelengths).

Thus for the fluorimetry studies, the two nanoparticle preparations having different folate levels (120 versus 1 folate molecule per nanoparticle) were incubated for 1 h at room temperature under constant mixing with folate-receptor-expressing lung carcinoma cells (A549) in suspension,²³ followed by cell harvesting via centrifugation. The resulting cell pellets were washed with 1X PBS to remove any unbound nanoparticles and finally reconstituted in 1 mL 1X PBS, allowing the comparison of total fluorescence emission per mL (Total FI_{mL}) among the various samples. Interestingly, fluorimetry studies revealed that the total fluorescence emission from the low cell density sample incubated with low-folate nanoparticles was higher than that of the corresponding high cell density sample (Figures 1A and 1B). This difference may be attributed to the higher number of recognizable epitopes in the cell suspension, as a result of the higher cell density (more cells more folate receptors), mediating the nanoparticles' quasi-dispersion with a concomitant reduction in cell-associated fluorescence.

Likewise, we assessed the high-folate nanoparticles interaction with A549 cells, by employing the same experimental approach. Contrary to what observed with the low-folate nanoparticles, fluorimetry studies demonstrated that under conditions of low cell density the total fluorescence emission was lower than that from the high cell density sample (Figures 1C and 1D). It is plausible that at low cell density the nanoparticles' higher valency may have facilitated the interaction of a given nanoparticle with multiple folate receptors found on the same cell. Consequently, this may have caused fewer high-folate nanoparticles interacting with a given cell, leading to less prominent cell-associated fluorescence. However, under high cell density, the high-folate nanoparticles multivalency could have promoted the nanoparticle's inter-cellular interaction with folate receptor epitopes found on adjacent cells in the nanoparticle's proximity, leading to enhanced fluorescence emission.

To further assess the interaction between our nanoparticles and cells, DLS was used to determine how the nanoparticle valency differentially mediates the dispersion state of the nanoparticles in solution under varying target cancer cell concentrations. In the absence of any cell in solution, the nanoparticles were highly dispersed as 100% of the nanoparticles had a diameter below 100 nm, as previously reported.²⁵ When the low folate nanoparticles were added to a suspension of cells at low cell density (10^3 A549 cells/mL), 23% of these nanoparticles formed large nanoparticle aggregates while only 77% remain dispersed (Table 1). In contrast, only 14% of the high-folate nanoparticles formed nanoparticle aggregates at the same cell density (10^3 A549 cells/mL), in accordance with our hypothesis (Table 1). As stated before, this may be attributed to the fact that the high-folate nanoparticles' increased valency can facilitate the interaction of a nanoparticle with multiple target receptors on the same cell, similar to what was observed through fluorescence spectroscopy (Figure 1C). Interestingly, when we increased the number of cells in suspension to 10^6 cells/mL, the population of low-folate nanoparticles adopting a clustered state decreased from 23% to 13%, whereas the population of clustered high-folate nanoparticles increased from 14% to 35% (Table 1). These changes are in line with the fluorimetry data, where similar changes were observed. Specifically, for the low-folate nanoparticles, DLS indicated a reduction by a factor of 1.77 versus 1.63 by fluorescence spectroscopy, whereas for the high-folate nanoparticles both methods provided comparable results (DLS increase by a factor of 2.5 vs 2.43 determined by fluorimetry). Taken together, the fluorimetry and dynamic light scattering results corroborate our model, and demonstrate that the nanoparticles' ligand valency modulates the differential interactions between folate nanoparticles. Hence, these distinct nanoparticle – cell associations in solution may facilitate different magnetic relaxation sensing dynamics and cell capturing capabilities.

The role of the nanoparticle valency in magnetic-relaxation-mediated mammalian cell detection

Detection with magnetic relaxation nanosensors (MRnS) is governed by the degree of nanoparticle association with a target.^{15,16} Based on the aforementioned data, we reasoned that there would be dramatic differences in the magnetic-relaxation-mediated cell detection, attributed to the nanoparticles' valency. We anticipated that nanoparticles with high valency, due to the multiple specific interactions between their carrying ligands and cell epitopes, may achieve better detection sensitivity and even single cancer cell quantification. This is critical, as it was recently demonstrated that even a single metastatic cancer progenitor cell can successfully induce tumor formation.²⁹

Specifically, we utilized the folate nanoparticle preparations (1 versus 120 folate moieties per nanoparticle) and the anti-FR ones (1 versus 4 antibody molecules per nanoparticle), in order to assess the detection performance of these nanosensors. To demonstrate the potential ability of our nanosensors to detect circulating cancer cells in clinical samples, we detected A549 cells

in blood diluted in phosphate buffered saline (PBS). In these studies, a stock cellular suspension of A549 cells was quantified using a hemocytometer, followed by the preparation of serial dilutions of the stock suspension in PBS-diluted blood. Subsequently, 10 μL aliquots of the resulting cellular suspensions were incubated with 190 μL of the corresponding nanoparticle working solution ($[\text{Fe}] = 0.01 \mu\text{g}/\mu\text{L}$) at room temperature, while monitoring the changes in spin-spin relaxation (ΔT_2) with a magnetic relaxometer operating at 0.47 T.

After a brief 1-hour-long incubation at room temperature under continuous mixing, distinct valency-dependent trends were observed (Figure 2A-D). We chose 1-hour-long incubation at room temperature in order to investigate the field applicability of our assay and its ability to provide fast and reliable results, whereas mixing of the samples minimized the possibility of nanoparticle internalization via folate-receptor-mediated endocytic uptake. An increase in the ΔT_2 was observed as the number of A549 lung carcinoma cells increased in solution when both high valency nanoparticles (high folate and high anti-FR antibody) were used (Figures 2A-B), whereas the opposite trend was observed for the nanoparticles with low ligand levels on their surface (decrease in ΔT_2 when the cell concentration increased) (Figures 2C-D). These results supported our hypothesis and were in line with the DLS and fluorimetry data. Specifically, as the ΔT_2 for high cell counts (>1000) of the low-folate nanoparticles was 1.5 – 1.7 ms and the ΔT_2 for a single cell detected by the high-folate nanoparticles was 2.5 ms, this may be attributed to the fact that 13% of the low folate nanoparticles interacted with cells at high cell density versus 14% of the high valency nanoparticles associated with cells at low cell density, as determined through DLS (Table 1).

Furthermore, our data suggest that in our previous report¹⁷ the observed decrease in ΔT_2 upon increase of the bacteria concentration was attributed to the nanoparticles' low antibody levels (low nanoparticle valency). This is corroborated by the detection pattern of the low-anti-FR nanoparticles (Figure 2D), exhibiting sigmoidal shape similar to our previous report using MAP bacteria and a corresponding low valency nanoparticle.¹⁷ Although the detection threshold of the low valency anti-FR nanoparticles was 10^4 cells, the low-folate nanoparticles were more sensitive and able to detect a single cell and quantify the target within the range of 1 to 10^3 cells, (Figures 2C). Most importantly, the high-folate nanoparticles were able to detect and quantify cells within an even wider dynamic range ($1 - 10^6$) (Figures 2A), outperforming the high anti-FR nanoparticles (Figures 2B) and demonstrating the versatility of small molecule ligands. Performing the magnetic relaxation studies at shorter incubation times (15 minutes) compromised data quality for the low-folate and both anti-FR nanoparticle preparations, leading to poor correlation coefficients (SI Table 1). However, the high-folate nanoparticles achieved good correlation coefficients ($R^2 > 0.9$) even after a 15-minute incubation, demonstrating the enhanced detection kinetics of the high-folate nanoparticles (Figure 3). Therefore in light of these results, valency plays a critical role in the detection profile of cancer cells using magnetic relaxation, as multivalency achieved via small molecules (folate) facilitates fast single cell detection in blood.

Next, we studied the specificity of our high-folate nanoparticles towards the folate receptor. Previously, it has been reported that antibody-carrying iron oxide nanoparticles can specifically detect bacteria,^{17,28} whereas negative controls of Protein-G iron oxide nanoparticles yielded no changes in the relaxation times.²⁸ First, we saturated the nanoparticles' solution with excess folate (10 mg/mL), and data indicated that the folate nanoparticles could not detect the lung carcinoma cells (A549) under these conditions, as seen by the concomitant absence of significant changes between the samples screened (Figure 4A). Likewise, saturation of the culture medium with excess folate (10 mg/mL) prevented the nanoparticles' interaction with the cells' folate receptors (FR), as indicated by the absence of fluorescence emission from the plasma membrane (SI Figure 6). Furthermore, we used cells that do not express the folate receptor (H9c2),²³ which when incubated with the nanosensors failed to induce any cell-

concentration-dependent changes in the solution's T2 times (Figure 4B). Thus, these data support the hypothesis that the folate nanoparticles interact specifically with the folate receptor at the plasma membrane of cells expressing this receptor, facilitating magnetic relaxation detection and fluorescence imaging.

Assessment of the ligand-modulated nanoparticle – bacterium interactions

After elucidating the role of nanoparticle valency in the nanoparticle – mammalian cell interaction in the target cells' magnetic relaxation detection trend and sensitivities, we investigated if this behavior applied to other systems. Particularly, we examined the role of the nanoparticle valency in the detection of bacteria. Hence for these studies, *Mycobacterium avium* spp. *paratuberculosis* (MAP) was used, which is smaller than mammalian alveolar cells (0.3 μm Vs 50 μm) and has dimensions comparable to other clinical relevant pathogens. Recently, we reported the magnetic-relaxation-mediated detection of MAP in complex media, observing that at low bacterial concentrations high ΔT_2 values were obtained, whereas at high bacterial concentrations ΔT_2 decreased.¹⁷ To elucidate this phenomenon, we prepared two MAP-specific nanosensors that carried different levels of anti-MAP antibodies. Specifically, two anti-MAP nanoparticle preparations with different valency levels were prepared, by varying the stoichiometric ratio of anti-MAP antibody to Protein-G nanoparticles (5 μg anti-MAP:250 μL Protein-G nanoparticles Vs 0.5 ng anti-MAP:250 μL Protein-G nanoparticles. The resulting anti-MAP nanoparticles had either high (4 anti-MAP molecules per nanoparticle on average) or low (1 anti-MAP molecule per nanoparticle on average) antibody levels per nanoparticle.

Through DLS, we observed that the anti-MAP nanoparticles yielded similar results to those obtained with the nanoparticles for the FR-expressing mammalian cancer cells (SI Table 2). Likewise, a valency-mediated differential behavior was also observed when we quantified MAP in whole milk using magnetic relaxation and the anti-MAP nanoparticle preparations, following literature available protocols.¹⁷ In particular, the low-anti-MAP nanoparticles exhibited high ΔT_2 at low bacterial concentrations, whereas at high bacterial concentrations ΔT_2 decreased (Figure 5A). These findings were in line with the aforementioned studies using low valency nanoparticles and our earlier report on bacteria detection.¹⁷ On the other hand, the high-anti-MAP nanoparticles demonstrated low ΔT_2 at low MAP concentrations, but as the target's concentration increased ΔT_2 increased (Figure 5B). Overall, the anti-FR and anti-MAP nanoparticles demonstrated similar quantifying capabilities, despite performing these studies in different matrices (blood Vs milk). Specifically, the high-anti-FR and high-anti-MAP nanoparticles can both quantify a region of two orders of magnitude ($10^4 - 10^6$ A549 cells and 10 – 1000 MAP CFUs respectively). Likewise, the low-anti-FR and low-anti-MAP nanoparticles can quantify roughly the same region of two orders of magnitude ($10^4 - 10^6$ A549 cells and ~30 – 1000 MAP CFUs), suggesting that this behavior may be attributed to the nature and dynamics of the antibody – antigen interaction.

Most importantly, these data suggest that the differential clustering of the nanoparticles is nanoparticle-valency-dependent, as neither the size of the ligands (small molecule Vs antibody) nor the size of the target (mammalian Vs bacterial cell) governs the interaction of the nanoparticles with a target. This is supported by the magnetic relaxation, DLS and fluorimetry data, indicating that more high-valency nanoparticles associate with cells at high cell density, as opposed to lower cell density. If the nanoparticle size governed the interaction with cells, one would have expected comparable levels of nanoparticles associating per target regardless of cell density and no differences between the low- and high-ligand nanoparticles detection patterns. Therefore, in light of these studies, our previously reported findings on bacteria detection¹⁷ were attributed to the nanoparticles' low valency. Taken together, the results of the

bacterial studies corroborate what was observed with the mammalian cells (A549) and further support our hypothesis.

The role of the nanoparticle valency in the magnetic isolation of cells

MRnS detection is a nondestructive technique performed in suspensions causing no damage to the cells. Therefore, we reasoned that after MRnS identification, cells could be magnetically isolated and used for further assays. Particularly, we hypothesized that nanoparticles with high valency would be able to magnetically isolate a higher number of cells, due to the contribution of multivalent interactions between the nanoparticles and their corresponding cellular targets. Considering the folate nanosensors' MRnS detection sensitivity and their robustness as they do not carry any heat-labile antibodies, we studied the performance of the folate nanoparticle preparations with low and high multivalency to magnetically isolate lung cancer cells with an LS25 MACS® column (Miltenyi Biotec). Acknowledging the need for circulating tumor cell isolation and propagation in order to use these cells for further assays,¹⁹ samples of equal population A549 cells in PBS-diluted blood, which had been screened through magnetic relaxation, were effectively isolated with either the low-folate ($[\text{Fe}] = 0.75 \mu\text{g}/\mu\text{L}$) or high-folate nanoparticles ($[\text{Fe}] = 0.75 \mu\text{g}/\mu\text{L}$) and then propagated (Figures 6A-B). However, the nanoparticles with lower valency captured fewer cells than the high-folate nanoparticles, as indicated by the corresponding cell counts after a 24 h propagation at 37 °C, 5% CO₂ (~45,000 cells for the low-folate nanoparticles Vs ~215,000 cells for the high-folate nanoparticles) (Figure 6C). In order to assess if the magnetic isolation of the cells compromised their cell viability, we utilized the MTT assay. Results indicated that the viability of the magnetically isolated cells was comparable to that of the corresponding controls (Figure 6D), demonstrating that the magnetic-relaxation-mediated detection and magnetic isolation of cells with the folate-carrying nanoparticles is non-destructive.

Next, we determined the magnetic cell-capturing efficiency of the high-folate nanoparticles, since these magnetic nanosensors exhibited enhanced detection sensitivity through magnetic relaxation and higher magnetic isolation of cells after analysis than the low-folate nanoparticles. Hence, after relaxation-mediated detection, the cell-containing PBS-blood samples were incubated with various iron concentrations of high-folate nanoparticles and then magnetically separated. Results showed that as little as 0.1 $\mu\text{g}/\mu\text{L}$ Fe of folate nanoparticles captured viable A549 cells, reaching a plateau after 0.75 $\mu\text{g}/\mu\text{L}$ Fe (Figure 7A-E). In contrast, when we used the non-functionalized nanoparticles, no cells were isolated (Figure 7F). Overall, these data indicate that our high-folate nanoparticle-based relaxation-mediated detection and subsequent magnetic isolation can be used in highly sensitive non-destructive assays.

Lastly, we utilized iron oxide nanoparticles' intrinsic peroxidase activity^{28,30,31} for the colorimetric high-throughput confirmation of the expression of folate receptor (FR) on the membrane of magnetically captured and propagated A549 cells (Figure 8A). For these studies non-fluorescent folate iron oxide nanoparticles were used. After magnetically isolating and re-growing the A549 cells, 500 of these cells were incubated with increasing concentrations of high-folate nanoparticles. We found that the A549 cells in the presence of H₂O₂ oxidized 3,3', 5,5'-tetramethylbenzidine (TMB) (Figure 8B) in a nanoparticle-concentration-dependent fashion, indicating that the cells were viable and still expressing the FR. At nanoparticle concentrations above 1.2 Fe $\mu\text{g}/\mu\text{L}$, the absorbance reached a plateau. The control A549 cells, which were magnetically isolated with folate nanoparticles but incubated with nonfunctionalized nanoparticles, demonstrated nominal peroxidase activity. This indicates that the contribution of nanoparticles used for magnetic isolation is nominal towards the overall peroxidase activity. In contrast, the non-folate-receptor-expressing H9c2 cells lacked any peroxidase activity (Figure 8B), as the folate nanoparticles did not associate with these cells. Through flow cytometry, we confirmed the expression of the FR in the magnetically captured

cells and its absence in the H9c2 control cells (SI Figure 7), thus corroborating the findings of nanoparticle-facilitated peroxidase assay (Figure 8B).

Discussion

Nature widely employs highly selective multivalent interactions.¹⁻¹¹ From enzymes and their substrates, to receptor – ligand pairs and antibody – antigen complexes, these associations are highly specific, despite being weaker than covalent interactions. For instance, the multivalent interaction between hemagglutinin of influenza virions and sialic acid moieties on bronchial epithelium cells mediates viral infection.⁷ Specifically, recent studies indicate that multivalency, apart from participating in the initial attachment of a pathogen (i.e. virus, toxin) to a target cell, is critical for uptake via complex, highly regulated endocytic processes, in addition to direct fusion.³² In line with these observations, recently, a multivalent gold nanoparticle conjugate has been reported to transform a weakly binding and biologically inactive small molecule into a potent multivalent nanoagent that effectively inhibits HIV-1 fusion to human T cells.³³

Considering the importance of multivalency on molecular recognition events, it is critical to assess its role in the sensitivity and detection pattern of novel nanoparticle-based diagnostic methods. Hence, in this report we addressed the fundamental question of how the nanoparticle valency affects the interaction of iron oxide nanoparticles with cells and what are the consequences in the magnetic-relaxation-mediated detection and magnetic isolation of these target entities. Our results indicate that nanoparticles with low valency switch from an assembled to a quasi-dispersed state as the target concentration increases, and this shift is accompanied with decrease in the ΔT_2 . On the other hand, nanoparticles with high valency move from a sparsely assembled to an extensive binding/clustered state, with a concomitant increase in ΔT_2 that is observed during this transition. Interestingly, similar results were obtained when mammalian or bacterial cells were used, suggesting that the previously reported differences in the detection of bacterial cells were attributed to the different levels of antibodies conjugated to the nanoparticles.^{17,28} Additionally, the shift in the relaxation detection pattern is valency-regulated, as neither the matrix (blood Vs milk), the ligand size (folate Vs anti-FR), nor the nanoparticle's coating (herein polyacrylic acid Vs dextran in previous reports^{17,28}) affected the quantification trend. Hence, valency engineering should be a critical aspect in the synthesis of sensitive magnetic relaxation nanosensors and perhaps other nanoparticle-based diagnostic assays.

Another important element in the design of robust and affordable nanosensors is the utilization of non-labile and readily available probes. In our studies, nanoparticles with high small molecule valency (high-folate nanoparticles) facilitated single cell detection and quantification in whole erythrocyte-containing blood, outperforming their low valency counterparts (low-folate nanoparticles) and antibody-carrying nanosensors (low- or high-anti-FR nanoparticles). Therefore, as it was recently demonstrated that even a single metastatic cancer progenitor cell can successfully induce tumor formation,²⁹ high-folate carrying nanoparticles may be used for the early detection of tumor cells in blood that overexpress the folate receptor. Furthermore, as the iron oxide nanoparticles can be easily conjugated via “click chemistry”, other small molecules may be used for the synthesis of high-valency nanosensors, capable of detecting rare circulating tumor cell in blood that may express other biomarkers. Small molecules, apart from being cheaper and more robust than antibodies, can offer comparable specificity and can be easily utilized for the engineering of the nanoparticle valency, due to their minimal steric hindrance. Since small-molecule-carrying nanoparticles can sense single cells, as opposed to antibody-carrying nanoparticles, the wider utilization of small molecules in molecular diagnostics is expected. For instance, bacteria can be targeted with small molecules screened from combinatorial libraries, leading to the development of bacterium-specific small-

molecule-carrying nanoparticles, which can achieve reliable and sensitive detection at the points-of-care and in the developing world.

Conclusion

We have demonstrated the role of iron oxide nanoparticle's ligand valency in (1) the rapid single cell detection of cancer cells in blood, (2) the magnetic isolation of cells for re-growth and further analyses, and (3) the corroboration of the presence of molecular targets in cultured cells' plasma membrane through a high-throughput cellular ELISA format. Finally, as we acknowledge the benefits of iron oxide nanoparticle-based assays and small molecule ligands, as well as the recent advancements in portable magnetic relaxation instrumentation,³⁴ we anticipate their broader use in the clinic and the field, expediting diagnosis and decision-making in cancer and infectious diseases.

Supplementary Material

Refer to Web version on PubMed Central for supplementary material.

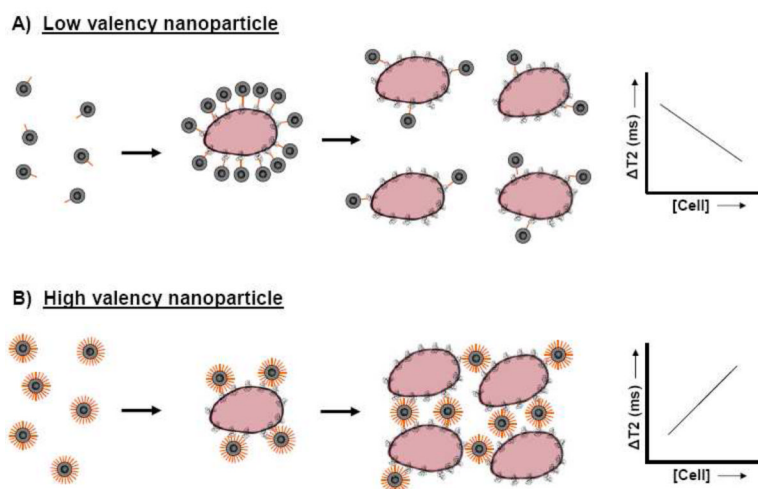
ACKNOWLEDGMENTS

The authors thank Dr. Saleh Naser (Burnett School of Biomedical Sciences, College of Medicine, UCF) for providing MAP and the anti-MAP antibody, Dr. James Hickman (Nanoscience Technology Center, UCF) for providing the fresh rat blood and the FITC-conjugated antibody, Mercedes Gonzales (Nanoscience Technology Center, UCF) for cell quantification, and Dr. Annette Khaled and Mounir Chehtane (Burnett School of Biomedical Sciences, College of Medicine, UCF) for their technical assistance in flow cytometry. This work was supported by the NIH grants CA101781 and GM084331 to JMP.

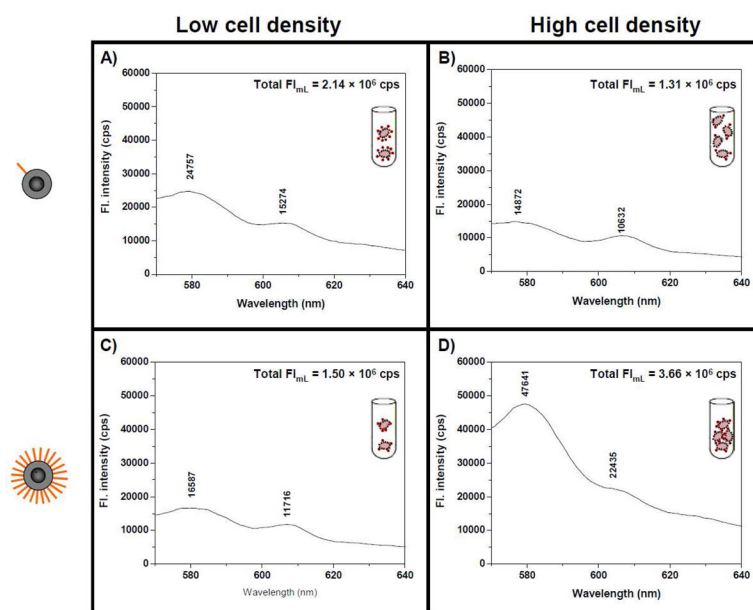
REFERENCES

1. Badjic JD, Nelson A, Cantrill SJ, Turnbull WB, Stoddart JF. *Acc Chem Res* 2005;38:723–32. [PubMed: 16171315]
2. Collins BE, Paulson JC. *Curr Opin Chem Biol* 2004;8:617–25. [PubMed: 15556405]
3. Greenspan NS. *Adv Cancer Res* 2001;80:147–87. [PubMed: 11034543]
4. Jo EK. *Curr Opin Infect Dis* 2008;21:279–86. [PubMed: 18448973]
5. Kiessling LL, Gestwicki JE, Strong LE. *Angew Chem Int Ed Engl* 2006;45:2348–68. [PubMed: 16557636]
6. Larsen M, Artym VV, Green JA, Yamada KM. *Curr Opin Cell Biol* 2006;18:463–71. [PubMed: 16919434]
7. Mathai M, Seok-Ki C, George MW. *Angewandte Chemie International Edition* 1998;37:2754–2794.
8. Mulder A, Huskens J, Reinhoudt DN. *Org Biomol Chem* 2004;2:3409–24. [PubMed: 15565230]
9. Ramsay AG, Marshall JF, Hart IR. *Cancer Metastasis Rev* 2007;26:567–78. [PubMed: 17786537]
10. Schwartz MA, DeSimone DW. *Curr Opin Cell Biol* 2008;20:551–6. [PubMed: 18583124]
11. Zutter MM. *Adv Exp Med Biol* 2007;608:87–100. [PubMed: 17993234]
12. Grimm J, Perez JM, Josephson L, Weissleder R. *Cancer Res* 2004;64:639–43. [PubMed: 14744779]
13. Kaittanis C, Nath S, Perez JM. *PLoS ONE* 2008;3:e3253. [PubMed: 18810269]
14. Perez JM, Grimm J, Josephson L, Weissleder R. *Neoplasia* 2008;10:1066–72. [PubMed: 18813356]
15. Perez JM, Josephson L, O'Loughlin T, Hogemann D, Weissleder R. *Nat Biotechnol* 2002;20:816–20. [PubMed: 12134166]
16. Perez JM, Simeone FJ, Saeki Y, Josephson L, Weissleder R. *J Am Chem Soc* 2003;125:10192–3. [PubMed: 12926940]
17. Kaittanis C, Naser SA, Perez JM. *Nano Lett* 2007;7:380–3. [PubMed: 17298004]
18. Cristofanilli M, Mendelsohn J. *Proc Natl Acad Sci U S A* 2006;103:17073–4. [PubMed: 17090687]

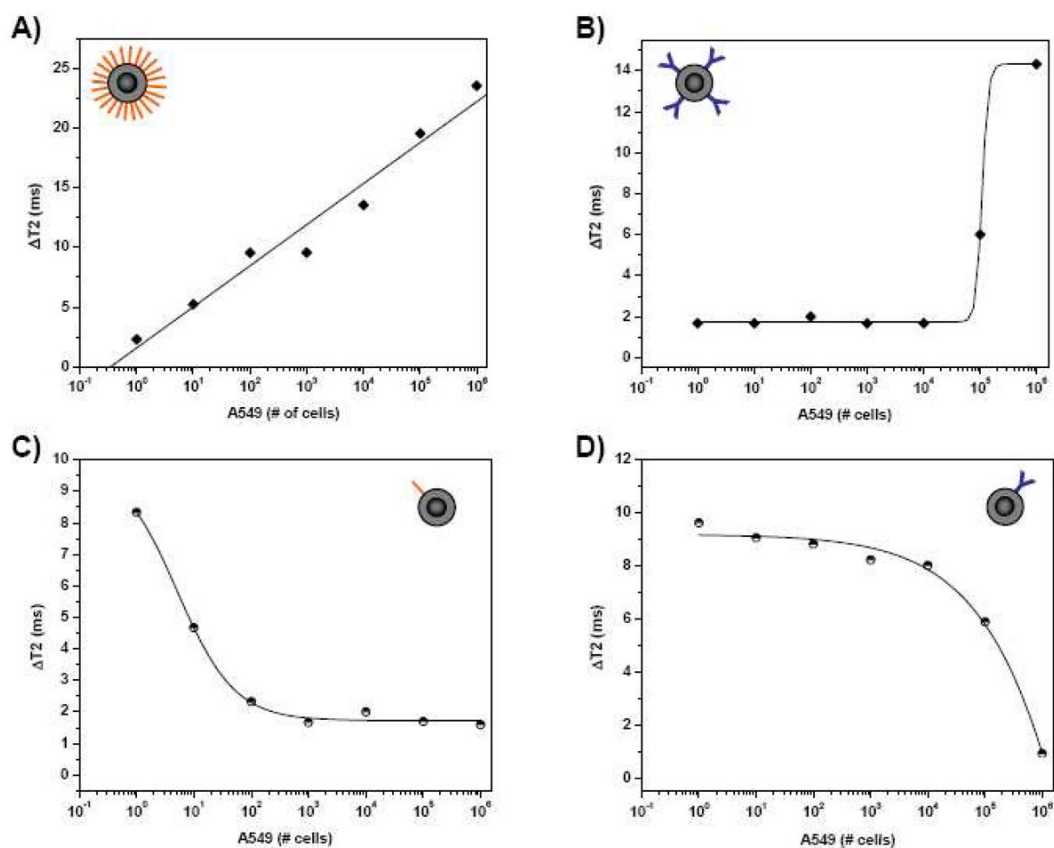
19. Nagrath S, Sequist LV, Maheswaran S, Bell DW, Irimia D, Ulkus L, Smith MR, Kwak EL, Digumarthy S, Muzikansky A, Ryan P, Balis UJ, Tompkins RG, Haber DA, Toner M. *Nature* 2007;450:1235–9. [PubMed: 18097410]
20. Sha MY, Xu H, Natan MJ, Cromer R. *J Am Chem Soc* 2008;130:17214–5. [PubMed: 19053187]
21. Bauer KD, de la Torre-Bueno J, Diel IJ, Hawes D, Decker WJ, Priddy C, Bossy B, Ludmann S, Yamamoto K, Masih AS, Espinoza FP, Harrington DS. *Clin Cancer Res* 2000;6:3552–9. [PubMed: 10999743]
22. Kraeft SK, Ladanyi A, Galiger K, Herlitz A, Sher AC, Bergsruud DE, Even G, Brunelle S, Harris L, Salgia R, Dahl T, Kesterson J, Chen LB. *Clin Cancer Res* 2004;10:3020–8. [PubMed: 15131038]
23. Parker N, Turk MJ, Westrick E, Lewis JD, Low PS, Leamon CP. *Anal Biochem* 2005;338:284–93. [PubMed: 15745749]
24. Alix-Panabieres C, Riethdorf S, Pantel K. *Clin Cancer Res* 2008;14:5013–21. [PubMed: 18698019]
25. Santra S, Kaittanis C, Grimm J, Perez JM. *Small*. 2009
26. Koch AM, Reynolds F, Kircher MF, Merkle HP, Weissleder R, Josephson L. *Bioconjug Chem* 2003;14:1115–21. [PubMed: 14624624]
27. Shen T, Weissleder R, Papisov M, Bogdanov A Jr, Brady TJ. *Magn Reson Med* 1993;29:599–604. [PubMed: 8505895]
28. Nath S, Kaittanis C, Ramachandran V, Dalal NS, Perez JM. *Chemistry of Materials* 2009;21:1761–1767.
29. Quintana E, Shackleton M, Sabel MS, Fullen DR, Johnson TM, Morrison SJ. *Nature* 2008;456:593–8. [PubMed: 19052619]
30. Gao L, Zhuang J, Nie L, Zhang J, Zhang Y, Gu N, Wang T, Feng J, Yang D, Perrett S, Yan X. *Nat Nanotechnol* 2007;2:577–83. [PubMed: 18654371]
31. Perez JM. *Nat Nanotechnol* 2007;2:535–6. [PubMed: 18654361]
32. Miyauchi K, Kim Y, Latinovic O, Morozov V, Melikyan GB. *Cell* 2009;137:433–44. [PubMed: 19410541]
33. Bowman MC, Ballard TE, Ackerson CJ, Feldheim DL, Margolis DM, Melander C. *J Am Chem Soc* 2008;130:6896–7. [PubMed: 18473457]
34. Lee H, Sun E, Ham D, Weissleder R. *Nat Med* 2008;14:869–74. [PubMed: 18607350]

**Scheme 1.**

The iron oxide nanoparticles's valency facilitates distinct magnetic relaxation sensing trends, which are modulated by the nanoparticle – target interactions. **A)** At low target concentrations, nanoparticles with low valency readily assemble on the target and cause large shifts in the ΔT_2 , whereas **B)** fewer nanoparticles with high valency interact per target resulting in lower ΔT_2 . At high target concentrations, the nanoparticles with **A)** low valency switch to a dispersed-like state with a concomitant ΔT_2 reduction, but **B)** the ones with high valency bind and cluster between multiple targets, facilitating prominent ΔT_2 changes.

**Figure 1.**

Distinct associations between fluorescent-labeled folate iron oxide nanoparticles and FR-expressing cells (A549) due to the nanoparticles' different valency. **A)** Low and **B)** high cell density A549 cells incubated with DiI-encapsulating low-folate nanoparticles. **C)** Low and **D)** high cell density A549 cells incubated with the corresponding high-folate nanoparticles. (The two primary fluorescence emission peaks for DiI are indicated, as well as the total fluorescence emission per mL (Total FI_{mL}) of the acquired spectra. Insets diagrammatically represent the interactions between cells and the nanoparticles in equal-volume samples.)

**Figure 2.**

Relaxation-mediated detection of cancer cells in PBS-diluted blood after a 60-min incubation, using **A)** high-folate nanoparticles, **B)** high-anti-FR nanoparticles, **C)** low-folate nanoparticles and **D)** low-anti-FR nanoparticles. (Means \pm SE; SE were within 1-2%, which are too small to be depicted)

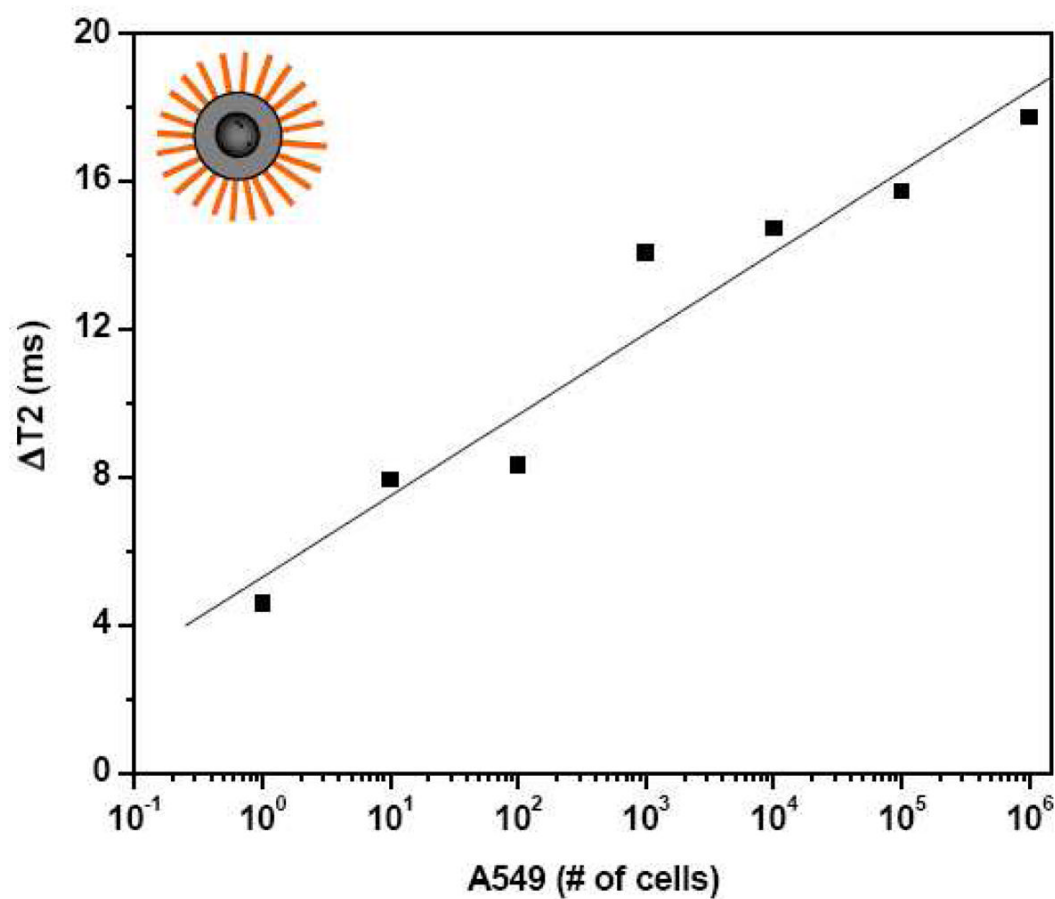


Figure 3. Relaxation-mediated detection of cancer cells in PBS-diluted blood after a 15-min incubation using high-folate nanoparticles. (Means \pm SE; SE were within 1-2%, which are too small to be depicted)

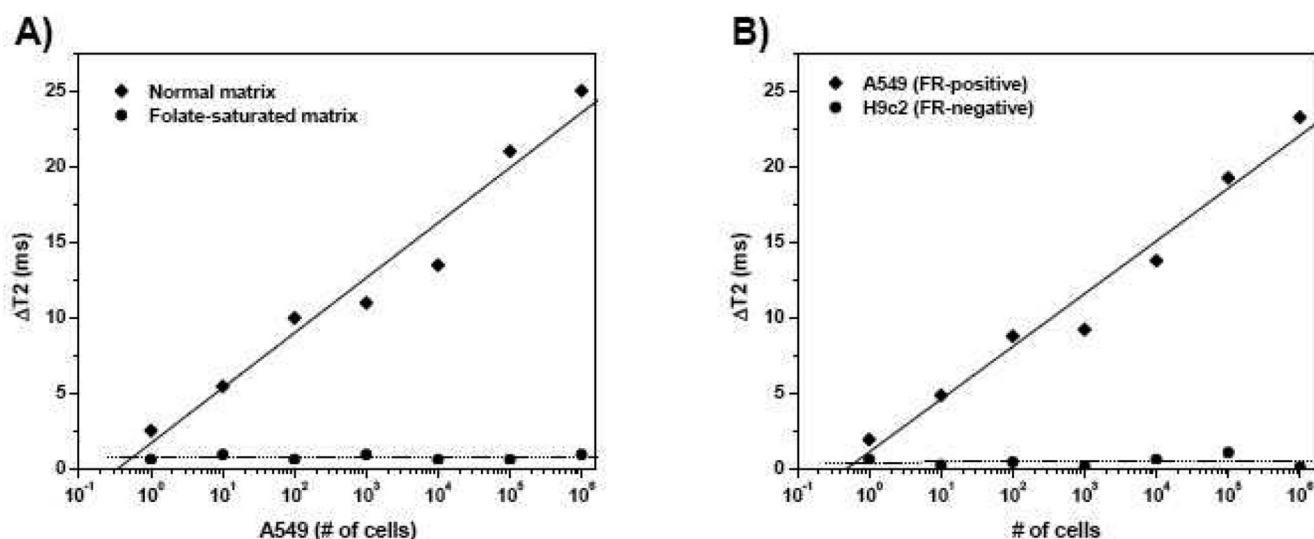


Figure 4. Determination of the folate nanoparticles' specificity through either (A) saturation of the matrix with excess folate or (B) folate-receptor (FR) negative cells. (Means \pm SE; SE were too small to be displayed (1-2%))

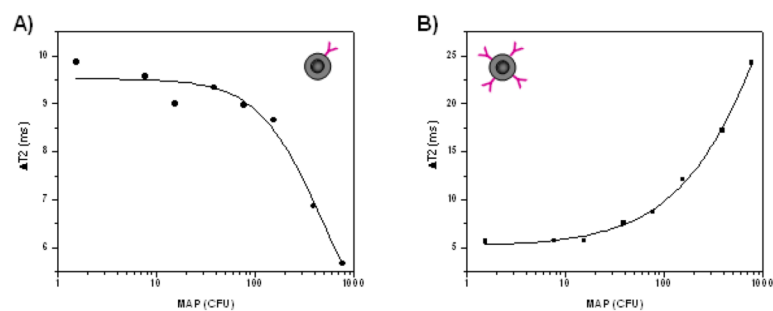


Figure 5. Relaxation-mediated detection of bacteria (MAP) in whole milk after a 60-minute incubation at room temperature. **A)** Low-anti-MAP ($R^2 = 0.97$) and **B)** high-anti-MAP ($R^2 = 0.99$) nanoparticles. (Means \pm SE; SE was within 1-2%, which cannot be depicted)

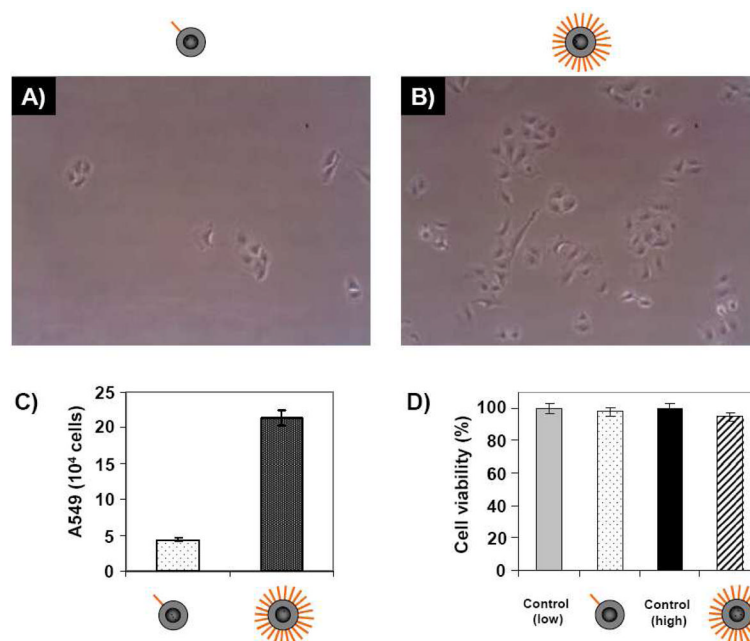


Figure 6. Nanoparticle-mediated magnetic isolation of FR-expressing cells. **A)** Low- and **B)** high-folate nanoparticles. **C)** Hemocytometer-mediated quantification of the captured cells after 24 h propagation at 37 °C, 5% CO₂, **D)** Cell viability of cells magnetically isolated with the low- and high-folate nanoparticles (Control low – 45,000 seeded cells, Control high – 215,000 cells). (Means \pm SE)

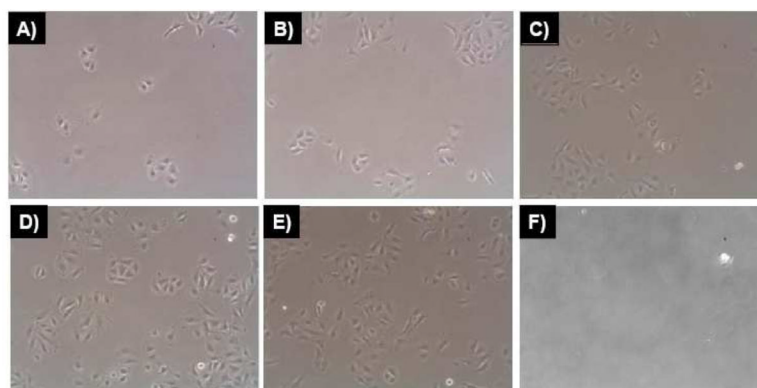


Figure 7.

Folate nanoparticles facilitate the magnetic isolation of FR-expressing tumor cells. The captured cells were grown at 37 °C, 5% CO₂ atmosphere, and visualized 24 h after isolation. Isolation of folate-receptor expressing cells with high-folate nanoparticles (**A.** 0.1, **B.** 0.25, **C.** 0.5, **D.** 0.75 and **E.** 1 µg/µL Fe). (**F**) Absence of cell growth when non-functionalized nanoparticles were used (1 µg/µL Fe).

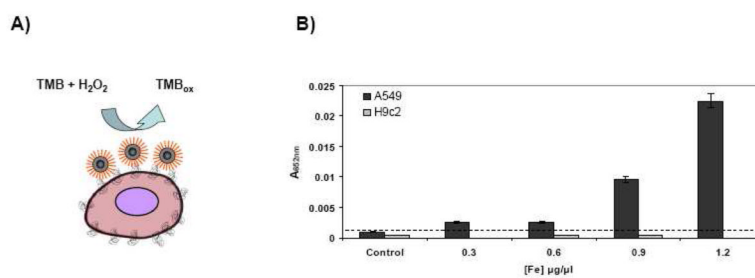




Figure 8.

A) Detection of FR-expressing cells using the folate nanoparticles' peroxidase activity. **B)** Carcinoma cells (500 A549 cells) oxidize TMB, whereas rat cardiomyocytes (H9c2) do not. Cells were treated with non-functionalized nanoparticles (1.2 $\mu\text{g}/\mu\text{L}$ Fe control) or different concentrations of high-folate nanoparticles (Means \pm SE).

Table 1Size distribution of the folate nanoparticles in the presence of various A549 concentrations. (Means \pm SE)

Nanoparticle	Diameter (nm)	Cell density	
		Low	High
	> 100	23 \pm 0.4%	13 \pm 0.5%
	< 100	77 \pm 0.3%	87 \pm 0.2%
	>100	14 \pm 0.2%	35 \pm 0.3%
	< 100	86 \pm 0.3%	65 \pm 0.5%